Macromolecules

ARTICLE

pubs.acs.org/Macromolecules

MALDI−TOF/TOF CID Study of Poly(phenylsulfidesulfone) Fragmentation Reactions

Anthony P. Gies,[†,‡,*] Sparkle T. Ellison,[§,⊥] Jon F. Geibel,[∥,#] and David M. Hercules[†]

[†]Department of Chemistry, Vanderbilt University, Nashville, Tennessee 37235, United States

[§]Department of Chemistry and Biochemistry, University of South Carolina, Columbia, South Carolina 29208, United States

[∥]Bartlesville Technology Center, Chevron Phillips Chemical Company, LP, Bartlesville, Oklahoma 74004, United States

Supporting Information

ABSTRACT: We report a combination of MALDI−TOF/TOF CID and Py−GC/MS to examine the fragmentation mechanisms of poly(phenylsulfidesulfone) (PPSS). Collision-induced dissociation (CID) fragmentation was initially used to examine the fragmentation pattern of PPSS and identify the preferred primary fragmentation pathways. On the basis of this information, a general fragmentation mechanism was developed and compared with the fragments generated by Py−GC/MS. These mechanisms were then compared with those of polysulfone (PSF) and poly(phenylsulfone) (PPSF), from our previous CID studies, to further refine our general fragmentation mechanism for poly(arylsulfone)s. Also, Py−GC/MS studies identified a total of eight sulfone-containing fragments; two of which have been observed in our previous study of PSF, while the remaining six represent new species which have not been previously reported for poly(arylsulfone)s. The identification of sulfone moieties in the Py−GC/MS of PPSS indicates that the phenyl-sulfide linkage, like that of the isopropylidene group found in polysulfone, may increase the stability of the polymer. Our study indicates that all three poly(arylsulfone)s preferentially cleave at the phenyl−sulfone bond, followed by the phenyl−oxygen or phenyl−sulfide bond, depending on which is present.

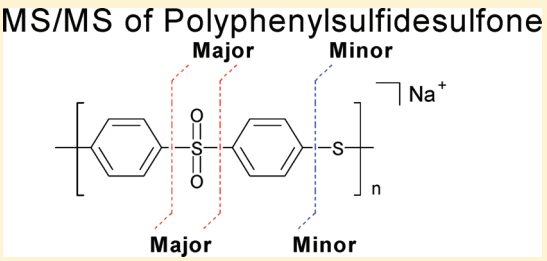

INTRODUCTION

Polyarylsulfones (PAS) are a unique family of thermoplastics that are distinguishable from most aromatic polymers by the presence of a para-linked diarylsulfone in the backbone. These polymers have three distinct performance characteristics that set them apart from other aromatic polymers: high glass transition temperatures, long-term thermal oxidative endurance, and high temperature melt thermal stability.[1,2] Further, the degradation pattern of a polymer is an important characteristic to consider when choosing a polymer for product manufacturing, which is the motivation behind this present study.

Analytical pyrolysis has been the traditional method employed to study the degradation of high-temperature polymeric materials, which are difficult to fragment and study by any other means. A number of thermal degradation studies of polysulfones (PSF), poly(ether sulfone)s (PES), and their blends or modifications have been published.[3−10] These studies have focused on the use of pyrolysis−gas chromatography/mass spectrometry (Py−GC/MS), Py−GC with flame ionization (FID) or flame photometric detection (FPD), and thermal gravimetric analysis (TGA) to analyze PAS degradation products. However, the combination of MALDI−TOF/TOF CID fragmentation and Py−GC/MS was able to shed new light on the fragmentation reaction mechanisms of PSF[11] and PPSF[12] and lead to the development of a general degradation mechanism for poly(arylsulfone)s. Because there is minimal research literature on the subject of PPSS degradation and analysis, it would be helpful to understand how the stability of the sulfide linkage, in PPSS,[13] relates to the ether linkage, in polyarylethersulfones (i.e., PSF, PES, and PPSF).

In the present study, we combine MALDI TOF/TOF CID fragmentation with Py−GC/MS to examine the chemical structures of suspected arylthio metathesis products[14] found in model PPSS and test the generality of our poly(arylsulfone) degradation mechanisms. Based on CID identification of a PPSS main-chain weak link at the phenyl−sulfone bond (Ph−SO_2), we were able to further refine our previously reported poly(arylsulfone) fragmentation mechanisms[11,12] and obtain "fingerprint" identification of "suspect" species. This work presents evidence for the existence of: (1) arylthio metathesis reactions,[14] (2) NMP side reactions leading to PPSS end group modification,[14] and (3) low kinetic energy "venting" of SO_2 from PPSS.

EXPERIMENTAL SECTION

Poly(phenylsulfidesulfone) Synthesis. The model poly(phenylsulfidesulfone) (PPSS) samples used in this study were produced

Received: March 11, 2011
Revised: June 8, 2011
Published: June 17, 2011

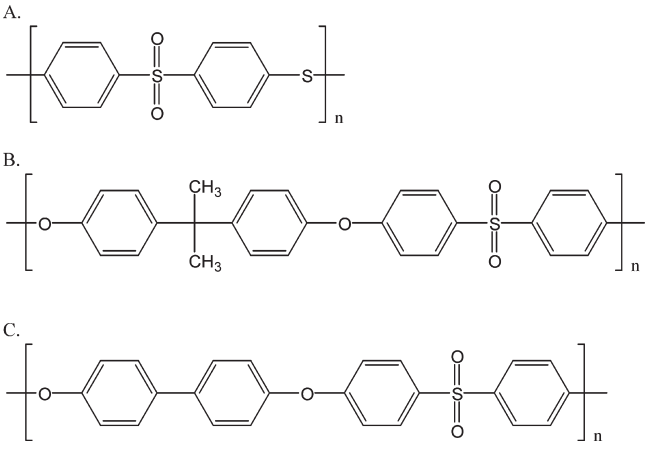

Figure 1. Structures of the repeat units for (A) poly(phenylsulfidesulfone) (PPSS), (B) polysulfone (PSF), and (C) poly(phenylsulfone) (PPSF).

by the Edmonds-Hill process,[15] with the exceptions of the use of 4,4′-dichlorodiphenyl sulfone and polymerization temperatures 60 °C cooler than for poly(*p*-phenyl sulfide) (PPS) and were supplied by Chevron Phillips Chemical Company, LP, Bartlesville, OK. The experimental conditions (i.e., monomer reaction ratios) were chosen to produce the desired end groups and degree of polymerization.[16] The structure of the polymer repeat unit was assumed to be that shown in Figure 1A. Also, the structural repeat units of polysulfone (PSF) and poly(phenylsulfone) (PPSF) are shown in Figure 1, parts B and C, respectively.

MALDI−TOF/TOF CID Measurements. All samples were analyzed using an Applied Biosystems 4700 Proteomics Analyzer MALDI−TOF/TOF MS (Applied Biosystems, Framingham, MA) equipped with a 355 nm Nd:YAG laser. All spectra were obtained in the positive ion mode using an accelerating voltage of 8 kV for the first source and 15 kV for the second source and a laser intensity of ∼10% greater than threshold. The grid voltage, guide wire voltage, and delay time were optimized for each spectrum to achieve the best signal-to-noise ratio. The collision energy is defined by the potential difference between the source acceleration voltage and the floating collision cell; in our experiments this voltage difference was set to 1 kV. Air was used as a collision gas at pressures of 1.5×10^{-6} and 5×10^{-6} Torr (which will later be referred to as "low" and "high" pressure, respectively). All spectra were acquired in the reflectron mode with a mass resolution greater than 3000 fwhm; isotopic resolution was observed throughout the entire mass range detected. External mass calibration was performed using protein standards from a Sequazyme Peptide Mass Standard Kit (Applied Biosystems) and a three-point calibration method using angiotensin I (m = 1296.69 Da), ACTH (clip 1−17) (m = 2093.09 Da), and ACTH (clip 18−39) (m = 2465.20 Da). Internal mass calibration was subsequently performed using a PEG standard (M_n = 2000; Polymer Source, Inc.) to yield monoisotopic masses exhibiting a mass accuracy better than $\Delta m = \pm 0.05$ Da. The instrument was calibrated before every measurement to ensure constant experimental conditions.

All samples were run in dithranol (Aldrich) doped with sodium trifluoroacetate (NaTFA, Aldrich). The samples were initially prepared using the evaporation−grinding method (E−G method) in which a 2 mg sample of poly(phenylsulfidesulfone) was ground to a fine powder using an agate mortar and pestle. Then molar ratios (with respect to the moles of polymer) of 25 parts matrix and one part cationizing agent (NaTFA) were added to the finely ground polymer along with 60 μL of distilled tetrahydrofuran (THF, Fisher). The mixture was ground until the THF evaporated after which the residue that had accumulated on the sides of the mortar was pushed down to the bottom of the vessel. The mixture was then ground again to ensure homogeneity. A sample of the mixture was then pressed into a sample well by spatula on the MALDI sample plate. Additional MALDI samples were prepared using the dried−droplet method (D−D method) with weight (mg) ratios of 50:10:1 (dithranol:polymer:NaTFA) in THF. After vortexing the mixture for 30 s, 1 μL of the mixture was pipetted onto the MALDI sample plate and allowed to air-dry at room temperature. MS and MS/MS data were processed using the Data Explorer 4.9 software (Applied Biosystems).

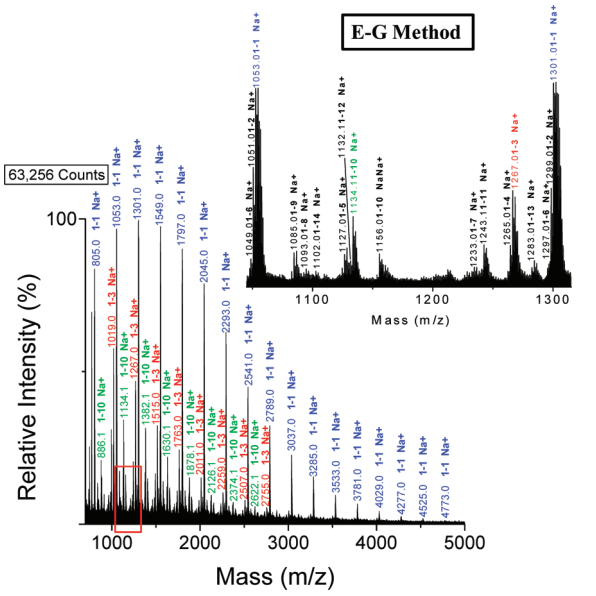

Figure 2. MALDI−TOF mass spectrum for PPSS, obtained using the E−G method.

Py−GC/MS Measurements. Polyphenylsulfidesulfone samples were analyzed using a Pyroprobe 2000 heated filament pyrolyzer (CDS Analytical, Oxford, PA) interfaced to an HP G1800C GC/MSD instrument (Palo Alto, Ca) (electron ionization −70 eV) via a CDS 1500 valve interface (CDS Analytical, Oxford, PA), kept at a constant temperature of 270 °C. The injection port and transfer line temperatures were both set at 270 °C. A 0.5 mg polymer sample and quartz wool (to prevent nonvolatile components from escaping the sample tube) were placed into a quartz sample tube; the tube was positioned inside the coil filament and allowed to purge under helium for 3 min in the pyrolysis interface. The pyrolyzer coil was then heated to 900 °C at a rate of 20 °C/ms and held for 10 s. The mass spectrometer was scanned from 40 to 500 Da. After obtaining the GC/MS, the quartz insert was removed from the pyrolyzer coil and flame cleaned. Additional measurements were made at pyrolysis temperatures of 650 and 1200 °C. However, 900 °C proved to be the most useful temperature for PPSS pyrolysis. The separation was performed using a 30 m (0.25 mm i.d. and 0.25 μm film thickness) HP-5 MS capillary column (Agilent, Palo Alto, CA). The column oven temperature was programmed to start at 50 °C for 3 min, ramp at 7.0 °C/min for 31.50 min, and held at 270 °C for 4.50 min, for a total heating cycle of 39 min.

RESULTS AND DISCUSSION

Previous Py−GC/MS studies have reported mechanistic information for the thermal degradation of polysulfones (PSF) and poly(ether sulfone)s (PES),[3,9,10] but, to date none have studied the thermal degradation of poly(phenylsulfidesulfone) (PPSS). For our study, we compared data from unimolecular fragmentation, by MS/MS, to the multimolecular free radical reactions of Py−GC/MS. MS/MS data will be presented first, followed by the results from Py−GC/MS analysis, which include fragmentation

Table 1. Structural Assignments for Peaks in the MALDI−TOF Mass Spectrum reported in Figures 2 and 3

Species	Structure (M)	$(M+Na)^+$ (Da)
1-1	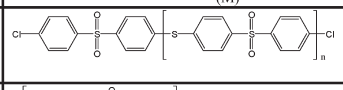	557.0 (n = 1) 805.0 (n = 2) 1053.0 (n = 3) 1301.0 (n = 4) ..... 7997.0 (n = 31)
1-2	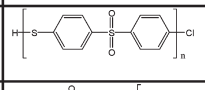	555.0 (n = 2) 803.0 (n = 3) 1051.0 (n = 4) 1299.0 (n = 5) ..... 7995.0 (n = 32)
1-3	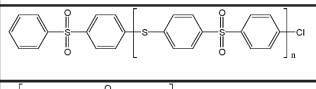	523.0 (n = 1) 771.0 (n = 2) 1019.0 (n = 3) 1267.0 (n = 4) ..... 7963.0 (n = 31)
1-4	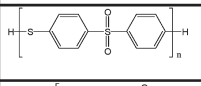	521.0 (n = 2) 769.0 (n = 3) 1017.0 (n = 4) 1265.0 (n = 5) ..... 7961.0 (n = 32)
1-5	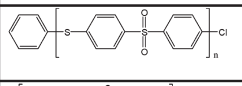	631.0 (n = 2) 879.0 (n = 3) 1127.0 (n = 4) 1375.0 (n = 5) ..... 7823.0 (n = 31)
1-6	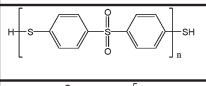	553.0 (n = 2) 801.0 (n = 3) 1049.0 (n = 4) 1297.0 (n = 5) ..... 7993.0 (n = 32)
1-7	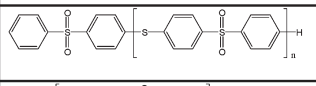	737.0 (n = 2) 985.0 (n = 3) 1233.0 (n = 4) 1481.0 (n = 5) ..... 7929.0 (n = 31)
1-8	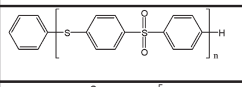	597.0 (n = 2) 845.0 (n = 3) 1093.0 (n = 4) 1341.0 (n = 5) ..... 7789.0 (n = 31)
1-9	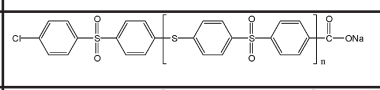	589.0 (n = 1) 837.0 (n = 2) 1085.0 (n = 3) 1333.0 (n = 4) ..... 7781.0 (n = 30)
1-10	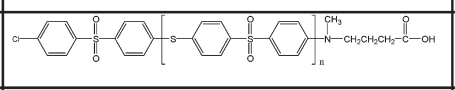	638.1 (n = 1) 886.1 (n = 2) 1134.1 (n = 3) 1382.1 (n = 4) ..... 7830.1 (n = 30)
1-11	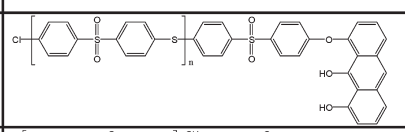	499.1 (n = 0) 747.1 (n = 1) 995.1 (n = 2) 1243.1 (n = 3) ..... 7691.1 (n = 29)
1-12	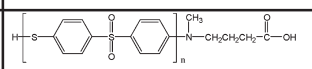	636.1 (n = 2) 884.1 (n = 3) 1132.1 (n = 4) 1380.1 (n = 5) ..... 7828.1 (n = 31)
1-13	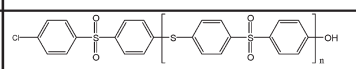	539.0 (n = 1) 787.0 (n = 2) 1035.0 (n = 3) 1283.0 (n = 4) ..... 7731.0 (n = 30)
1-14	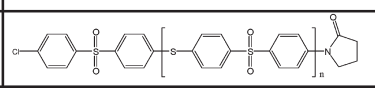	606.0 (n = 1) 854.0 (n = 2) 1102.0 (n = 3) 1350.0 (n = 4) ..... 7798.0 (n = 30)

mechanisms and the preferential order of bond cleavage. A comparison of these mechanisms with those of PSF[11] and poly(phenylsulfone) (PPSF)[12] is included.

MALDI−TOF/TOF CID. Figure 2 displays a representative MALDI spectrum of PPSS, prepared using the E-G method. The identities of the labeled peaks, in Table 1, reveal a wealth of information about the mass, structure, and end-groups of PPSS molecules generated by synthesis and postsynthesis chemical treatments. Additionally, structures 1−9, 1−10, 1−12, 1−13, and 1−14 indicate end group modification, which are caused by sodium *N*-methyl-2-aminobutanoate (SMAB) reactions with PPSS (previously reported in PPS synthesis).[14,17−19] SMAB is necessary for the solvation of NaSH during PPS and PPSS synthesis.[19] These NMP modified structures can also be produced through displacement reactions along the PPSS backbone, much like the arylthio metathesis reactions in PPS.[14] This process is analogous to transesterification reactions that are commonly observed in polyester synthesis. The incoming nucleophile is

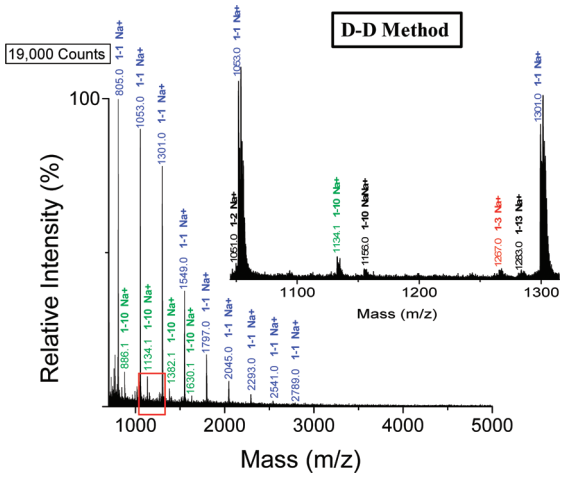

Figure 3. MALDI−TOF mass spectrum for PPSS, obtained using the D−D method.

predominantly a sulfone or sulfide, but, other nucleophiles are present in the PPSS reaction mixture (oxygen and nitrogen nucleophiles, for example). Incoming nucleophiles, involving oxygen or nitrogen, cleave sulfone linkages; yielding a net reduction in MW and production of "NMP modified" end groups (i.e., structures 1−9, 1−10, 1−12, 1−13, and 1−14). This displacement reaction could explain why NMP modified structures are primarily observed in the low mass region of the MALDI spectra (Figure 2). It should be noted that the dithranol end group modification on structure 1−11, is an artifact of the MALDI process. The cholorine end groups in PPSS are strongly activated by the sulfone group, making them susceptible to attack from one of the three hydroxyl groups on dithranol.

In order to understand the degradation reactions of PPSS, it is necessary to select individual precursor ions for CID fragmentation. Structure 1−1 (shown in Table 1) is an ideal precursor ion for two main reasons: (1) it shows the most intense mass peaks in Figure 2 and (2) its two chlorine end groups can greatly simplify the interpretation of its CID fragmentation pattern. However, inspection of the inset shown in Figure 2 reveals two problems with the dichloro-capped structure 1−1 precursor ions: (1) the chloro-thiol end-capped structure 1−2 is only 2 Da lower than the precursor ion of interest (structure 1−1) and (2) the chlorine end group on structure 1−2 yields an M+2 isotope that is isobaric with the first chlorine isotope of structure 1−1. These two issues make it impossible to individually select structure 1−1 for fragmentation without the possibility of structure 1−2 complicating the fragmentation pattern. In an effort to overcome this problem, we chose to exploit the solubility issues associated with the different PPSS end groups and to use the conventional dried-droplet MALDI sample preparation method for our initial CID studies. Figure 3, shows that using the D−D method with THF as the solvent greatly simplifies the MALDI spectrum by selectively dissolving the dichloro-capped structure 1−1 and eliminating all thiol-capped structures from the MALDI spectrum. This experiment effectively illustrates how solubility issues can be used to advantage. However, by so doing the mass range that can be investigated is limited to much lower molecular weights.

The next step was to conduct CID fragmentation on a variety of poly(phenylsulfidesulfone) precursor ions. However, it was discovered that molecular masses above 2000 Da did not generate usable CID spectra for PPSS. Although it would be desirable to

Table 2. Structural Assignments for Peaks in the MALDI–TOF/TOF Mass Spectrum Reported in Figures 4–6

Species	Structure (M)	Na^+ (* = Carbocation with no Na+) M (Da)
2-1	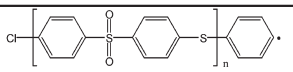	382.0 (n = 1) 630.0 (n = 2) 878.0 (n = 3) 1126.0 (n = 4) 1374.0 (n = 5) 1622.0 (n = 6)
2-2	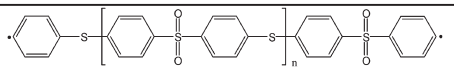	595.0 (n = 2) 843.0 (n = 3) 1091.0 (n = 4) 1339.0 (n = 5) 1587.0 (n = 6)
2-3	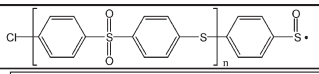	926.0 (n = 4) 1174.0 (n = 5) 1422.0 (n = 6) 1670.0 (n = 7)
2-4	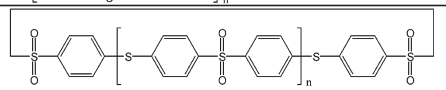	*808.0 (n = 2) 831.0 (n = 2) *1056.0 (n = 3) 1079.0 (n = 3) *1304.0 (n = 4) 1327.0 (n = 4) *1552.0 (n = 5) 1575.0 (n = 5)
2-5	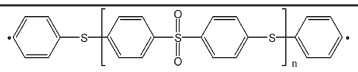	*184.0 (n = 0) 455.0 (n = 1) 703.0 (n = 2) 951.0 (n = 3) 1199.0 (n = 4) 1447.0 (n = 5)
2-6	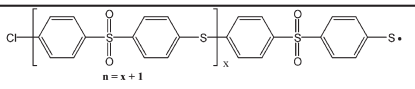	306.0 (n = 1) 554.0 (n = 2) 802.0 (n = 3) 1050.0 (n = 4) 1298.0 (n = 5) 1546.0 (n = 6)
2-7	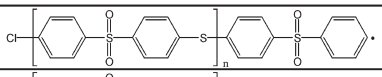	770.0 (n = 3) 1018.0 (n = 4) 1266.0 (n = 5) 1514.0 (n = 6)
2-8	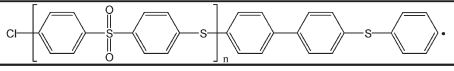	814.0 (n = 2) 1062.0 (n = 3) 1310.0 (n = 4) 1558.0 (n = 5)
2-Frag 1		87.0
2-Frag 2		134.0
2-Frag 3		* 172.0
2-Frag 4	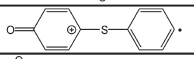	* 200.0
2-Frag 5	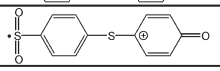	* 264.0 265.0 (H+)

examine PPSS molecular masses out to 5000 Da, the CID spectra obtained, yielded sufficient fragment information to study the degradation reactions and end group modifications of PPSS. Table 2 summarizes the masses of the fragment ion peak series observed in MALDI–TOF/TOF CID mass spectra from the dichlorine-capped poly(phenylsulfidesulfone) oligomer ions: 1053.0 Da (n = 3; Figure S1 in the Supporting Information section), 1301.0 Da (n = 4; Figure 4), 1549.0 Da (n = 5; Figure 5), 1797.0 Da (n = 6; Figure 6). All values listed are for sodium-cationized poly(phenylsulfidesulfone) ions, unless noted otherwise.

PPSS Precursor Structure 1–1. Figure 4 shows the MALDI–TOF/TOF CID spectrum for the dichlorine-capped PPSS structure with n = 4 (structure 1–1, 1301.0 Da). The precursor ion was selected from the MALDI spectrum shown in Figure 3. Inspection of the fragment ion peak intensities, in Figure 4, indicates that PPSS preferentially fragments at the Ph–SO_2 bond to generate primarily chloro–phenyl (species 2–1) capped fragments and a small amount of phenyl–phenyl (species 2–5), chloro–sulfoxide (species 2–3), and sulfone–sulfone (cyclic species 2–4) capped fragments. There also appears to be a small amount of chlorine end group loss, producing species 2–2, and random cleavage of the Ph–S bond, which results in the production of species 2–6 and 2–7. Species 2–8 can only be explained by a fragment ion containing a biphenyl linkage, which would indicate that SO_2 is "venting" from the PPSS main-chain.

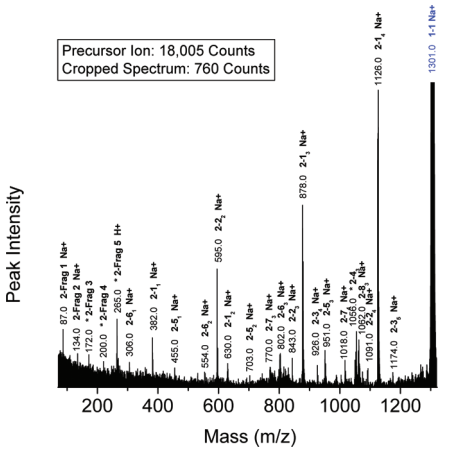

Figure 4. MALDI–TOF/TOF mass spectrum for linear PPSS (1301.0 Da precursor ion; n = 4) at a collision gas pressure of 5 × 10^{-6} Torr, representative of *medium* effective kinetic energy fragmentation.

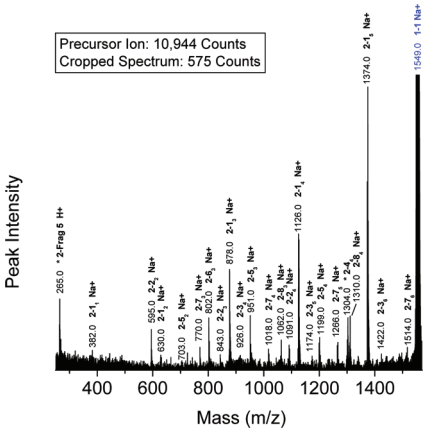

Figure 5. MALDI–TOF/TOF mass spectrum for linear PPSS (1549.0 Da precursor ion; n = 5) at a collision gas pressure of 5 × 10^{-6} Torr, representative of *medium/low* effective kinetic energy fragmentation.

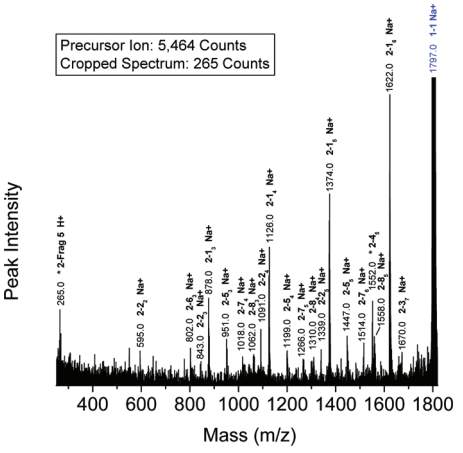

Figure 6. MALDI–TOF/TOF mass spectrum for linear PPSS (1797.0 Da precursor ion; n = 6) at a collision gas pressure of 5 × 10^{-6} Torr, representative of *low* effective kinetic energy fragmentation.

A mechanism for SO_2 extrusion from poly(ether sulfone) has been previously suggested by Montaudo et al.[6] Essentially, the

Scheme 1. TOF/TOF CID Fragmentation for Dichloro-Capped PPSS Oligomers

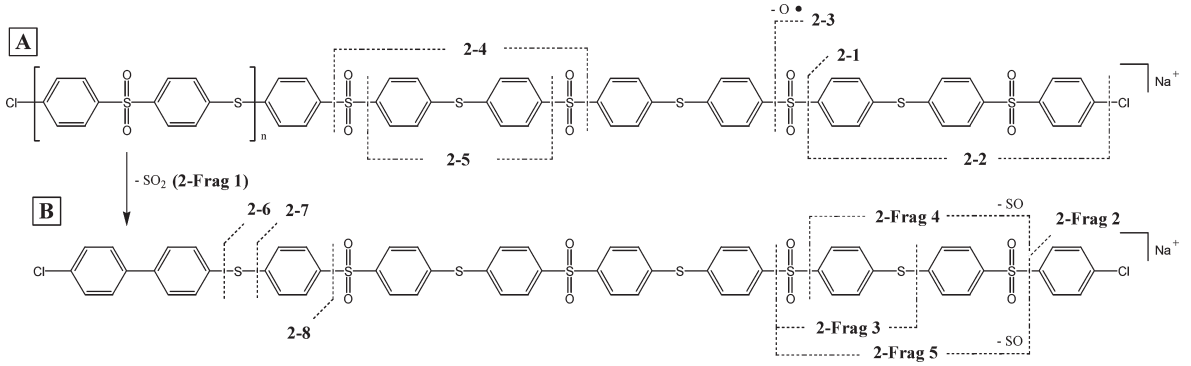

tetrahedral conformation of the diphenyl sulfone group (with interaction between the phenyl and sulfur electron orbitals) encourages intramolecular extrusion of SO_2 and direct formation of biphenyl linkages within the polymer backbone.[6]

Using the information above, we have presented a general PPSS fragment model, shown in Schemes 1 and 2, to explain the distribution of fragment ions observed in our PPSS CID fragmentation spectra (Figures 4−6). Later in our discussion, we will relate the low kinetic energy fragmentation pathways of MS/MS to the high kinetic energy conditions of pyrolysis (Schemes 3, 4, and 5).

First, consider the single bond cleavages of the Ph−SO_2 bond, as shown in Scheme 2A. Going from left-to-right we observed the following fragment ions (species 2−1): 382.0, 630.0, 878.0, and 1126.0 Da. Because the molecule is symmetrical, one observes the same pattern when going from right-to-left. These fragment ions represent the most intense mass peaks in the spectrum, especially at higher molecular masses. (This fragmentation is comparable to that of the most intense peaks observed in previous MS/MS studies of linear PSF[11] and PPSF.[12]) When a single Ph−SO_2 cleavage occurs, and the sulfone radical chain-end can lose an oxygen atom (Scheme 2B), producing fragment ions (species 2−3): 926.0 and 1174.0 Da. PPSS is capable of SO_2 "venting" (Scheme 2C), eliminating sulfur dioxide, as discussed above, from the PPSS main-chain, with concomitant formation of a biphenyl linkage in the PPSS backbone. This appears to be a low energy pathway, by which, PPSS can dissipate internal energy, and inhibit extensive fragmentation. This process produces the fragment ion observed at 1062.0 Da (species 2−8). It should be noted that the biphenyl linkage introduces a PPSS weak-link at the Ph−S bonds adjacent to the biphenyl linkage. Fragmentation of this Ph−S weak-link produces the following ions (species 2−7): 770.0 and 1018.0 Da.

When sufficient energy is present, multiple bond cleavages can occur at the Ph−SO_2 bonds (Scheme 2D) to produce the fragment ions (species 2−5) at 455.0, 703.0, and 951.0 Da. An additional multibond fragmentation mechanism of interest is shown in Scheme 2E, which represents the loss of a chlorine end group and cleavage of a Ph−SO_2 bond. From left-to-right (in the lower portion of Scheme 2E) we observe the following ions (species 2−2): 595.0, 843.0, and 1091.0 Da. Fragmentation from right-to-left (the upper portion of Scheme 2E) produces species 2−1. Further, under high energy conditions, fragmentation of the Ph−S bond can occur (Scheme 2F), at a limited extent, to produce low intensity species 2−6 (306.0, 554.0, 802.0, and 1050 Da) and species 2−7 (522.0, 770.0, and 1018.0 Da) fragment ions.

Comparison of the CID fragmentation spectra of PPSS 1301.0 Da (Figure 4, high KE conditions) with PPSS 1549.0 Da (Figure 5 − medium KE conditions) and PPSS 1797.0 Da (Figure 6, low KE conditions), reveals no change in the peak intensities of species 2−1. It is the most major species in all spectra. This is due to two reasons: (1) fragmentation of the Ph−SO_2 bond, as shown in Scheme 2A, is a low energy pathway and (2) species 2−1 is formed by five of the six fragmentation reactions shown in Scheme 2, parts A−E. Another low energy pathway arises from multiple main-chain breaks of the Ph−SO_2 bonds to form species 2−5. Its peak intensities increase as the effective KE decreases (*cf.*, Figures 4 and 6). Another possible route for the formation of species 2−5 would be the loss of SO_2 radical end groups from species 2−4, before it can form a stable cyclic structure. However, an intermediate species having only one SO_2 radical is not seen, so this is unlikely to be a major pathway for its formation. Furthermore, the peak intensities for species 2−4 (produced when two sulfone radical end groups "click" together to form a stable cyclic species) appear to remain constant under high and low KE conditions. It is also interesting to note that cyclic species 2−4 is found almost exclusively at peak mass M − 245 Da, in all of the CID spectra, produced when the two phenyl chloride end-caps "snap" off. Similarly, this was observed in our previous studies of PSF[11] and PPSF.[12] Presumably, these polymers are too rigid to allow the formation of smaller cyclic species.

The most interesting low energy fragmentation pathway appears to be SO_2 "venting" from the PPSS main-chain (Scheme 2C). For example, species 2−8 can only be explained by the formation of a biphenyl linkage in the PPSS fragment backbone. Its peak intensities increase with decreasing effective KE (*cf.*, Figures 4 and 6). Furthermore, the formation of a biphenyl linkage in the PPSS backbone forms a previously described weak link[12,13] that results in the formation of species 2−7. Note that the peak intensities for species 2−7 also increase with decreasing effective KE (*cf.*, Figures 4 and 6). Species 2−6 also has the potential to be formed due to cleavage of the Ph−S bond directly adjacent to the biphenyl linkage. However, its peak intensities dramatically decrease with decreasing kinetic energy—indicating that species 2−6 is predominantly formed by high KE fragmentation of the Ph−S bond, as shown in Scheme 2F. Note that, when a biphenyl linkage is present, preferential cleavage occurs at the Ph−S bond β to the biphenyl group. This fragmentation mechanism is consistent with our previous CID fragmentation studies of PPS possessing dibenzothiophene linkages.[13] Therefore, we would expect to see formation of species 2−7 (*not* species 2−6) by this mechanism. Since, species 2−7 appears to be formed under low KE conditions,

dx.doi.org/10.1021/ma200564f |*Macromolecules* 2011, 44, 5093–5104

Scheme 2. Species Specific TOF/TOF CID Fragmentation Reactions for Dichloro-Capped PPSS (1301.0 Da; n = 4)

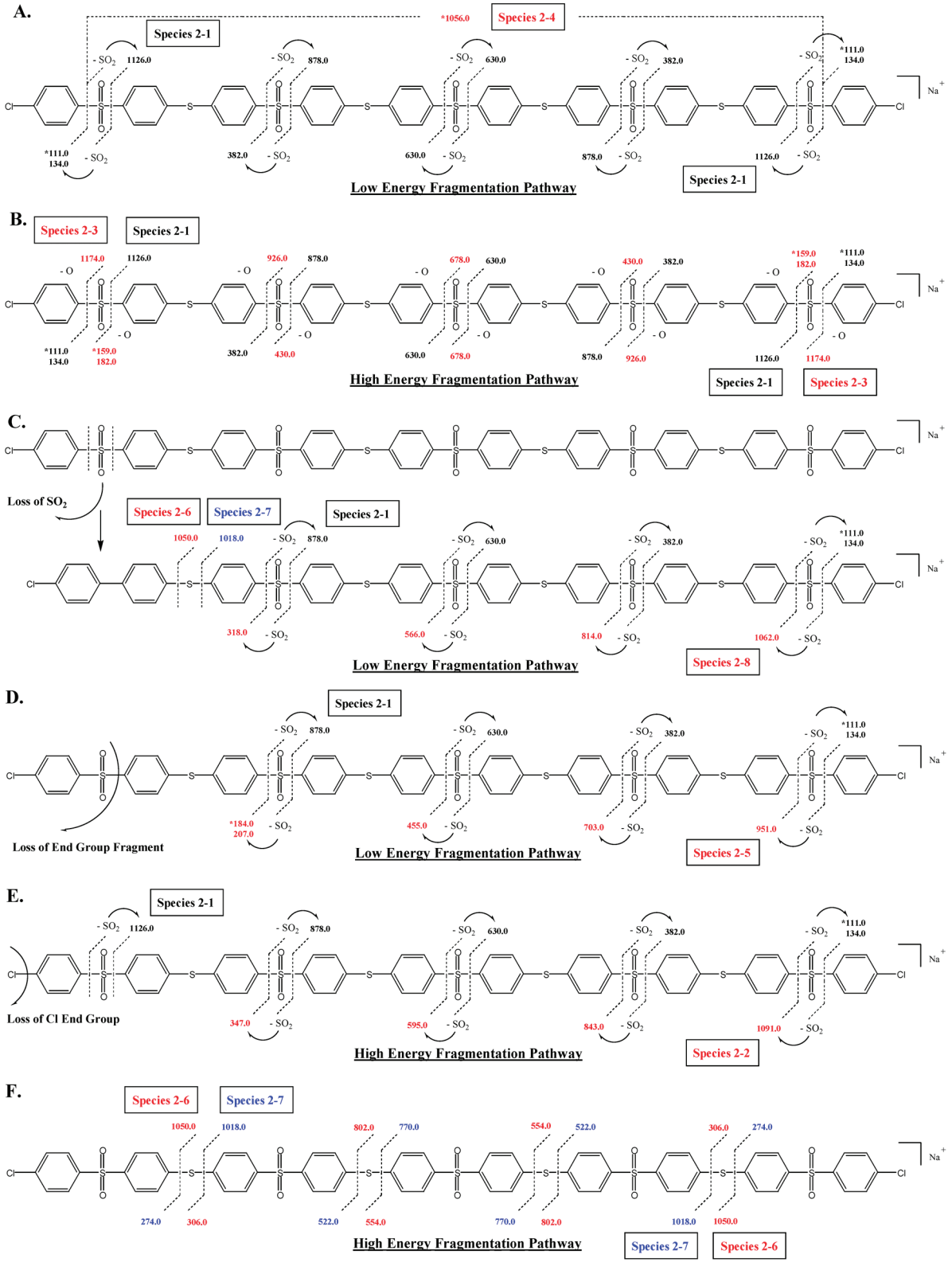

this would rule out any major contribution from high energy β-scission reactions from species 2−1.

The last fragmentation reactions we will discuss occur under high energy conditions; an example is the formation of species 2−2. This species can be formed through cleavage of a Ph−SO_2 bond and an additional chain break of a Ph−S bond or end group loss of a chlorine atom. Inspection of Figures 4, 5, and 6 shows that the peak intensities of species 2−2 decrease with decreasing

dx.doi.org/10.1021/ma200564f |*Macromolecules* 2011, 44, 5093–5104

Scheme 3. Major Pyrolysis Fragmentation Mechanisms of Poly(phenylsulfidesulfone)[a]

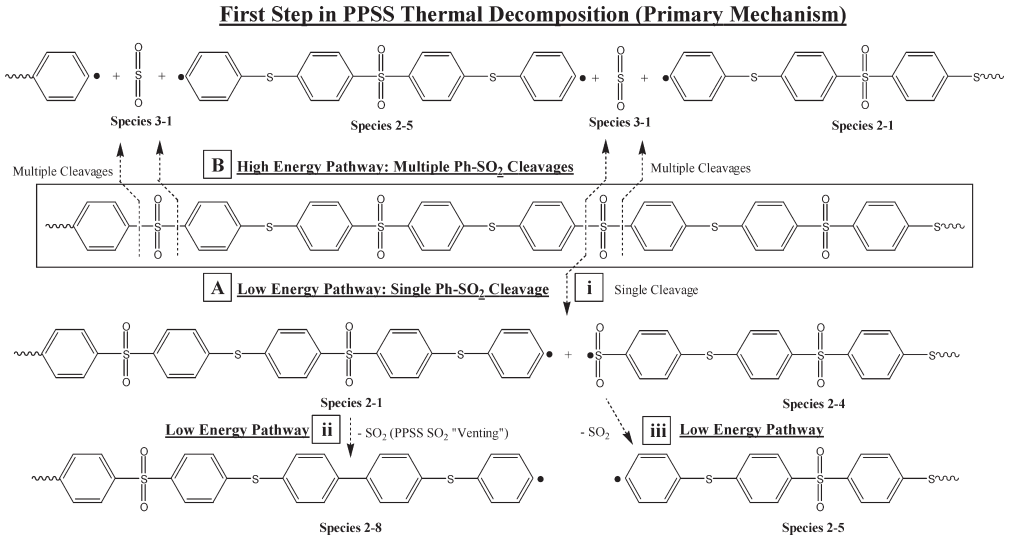

[a] Key: (A) Low-energy cleavage of a single Ph−SO_2 bond and (B) high-energy cleavage of multiple Ph−SO_2 main-chain bonds for production of species 2−1, 2−4, 2−5, 2−8, and 3−1.

Scheme 4. Secondary (High-Energy) Pyrolysis Fragmentation Mechanisms of Poly(phenylsulfidesulfone)[a]

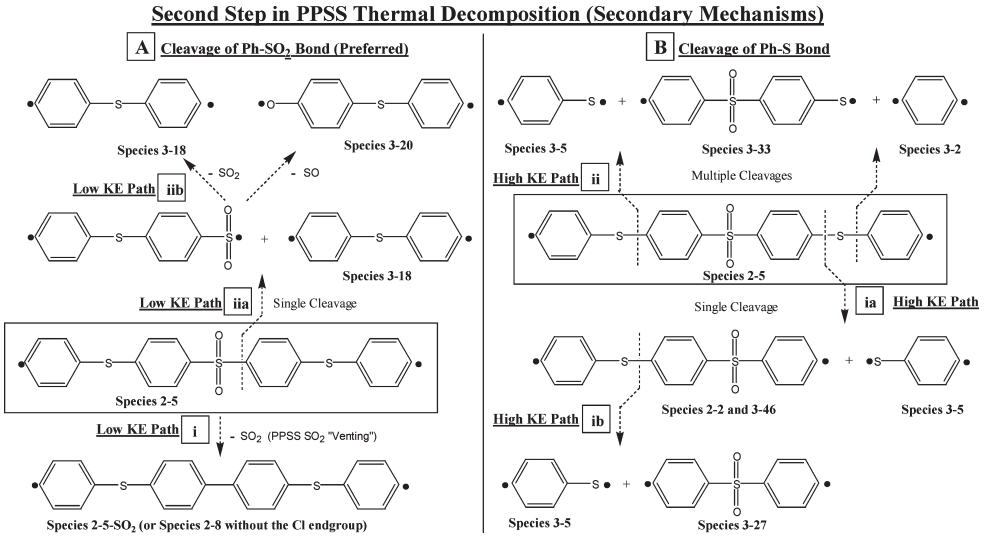

[a] Key: (A) Cleavage of the Ph−SO_2 bond to produce (i) 2-5-SO_2 or (ii) species 3−18 and 3−21. (B) Species 2−5 undergo single bond cleavages at the Ph−S Bond to produce (ia) species 3−5 and 2−2 (aka 3−46) and (ib) species 3−5 and 3−27 or (ii) undergo multiple cleavages of the Ph−S bond to produce species 3−2, 3−5, and 3−33. All fragment species are observed in Figure 7.

effective KE. In fact, the 2−2 species almost disappears in Figure 6. Other possible pathways for the formation of species 2−2 would include the following: (1) short-chain monomer reversion (i.e., loss of a benzenethiol group) reactions from species 2−5 and (2) species 2−7 undergoing cleavage of a Ph−SO_2 group. The last two high energy reactions occur due to fragmentation of the Ph−SO_2 bond followed by loss of an oxygen atom (species 2−3) and Ph−S bond (species 2−6). Since the origins of species 2−6 have already been presented above, we will finish our discussion of fragmentation reactions with species 2−3. Examination of the peak intensities of species 2−3, shows a dramatic decrease when going from high energy (Figure 4) to low energy (Figure 6) fragmentation conditions. It is also interesting to note that high molecular mass oxygen terminated fragment ions are not observed—only the sulfoxide capped species. Although, oxygen terminated fragments do appear at low molecular mass. For example, in Figure 4, addition of the mass peaks at 926.0 Da (species 2−3_4 Na^+), 265.0 Da (×2-Frag 5 H^+), and 134.0 (×2-Frag 2 Na^+) (subtracting the molecular masses of the H^+ and Na^+ cations from ×2-Frag 5 H^+ and ×2-Frag 2 Na^+) yields the molecular mass of the precursor ion: 1301.0 (structure 1−1 Na^+). Similarly, species ×2-Frag 4 (200.0 Da) and SO_2 (64.0 Da) could be substituted in place of species ×2-Frag 5 H^+ (265.0 Da minus 1 Da for the H^+ atom yields 264.0 Da) to yield the mass of

dx.doi.org/10.1021/ma200564f |*Macromolecules* 2011, 44, 5093–5104

Scheme 5. Tertiary (High-Energy) Pyrolysis Fragmentation Mechanisms of Poly(phenylsulfidesulfone):[a]

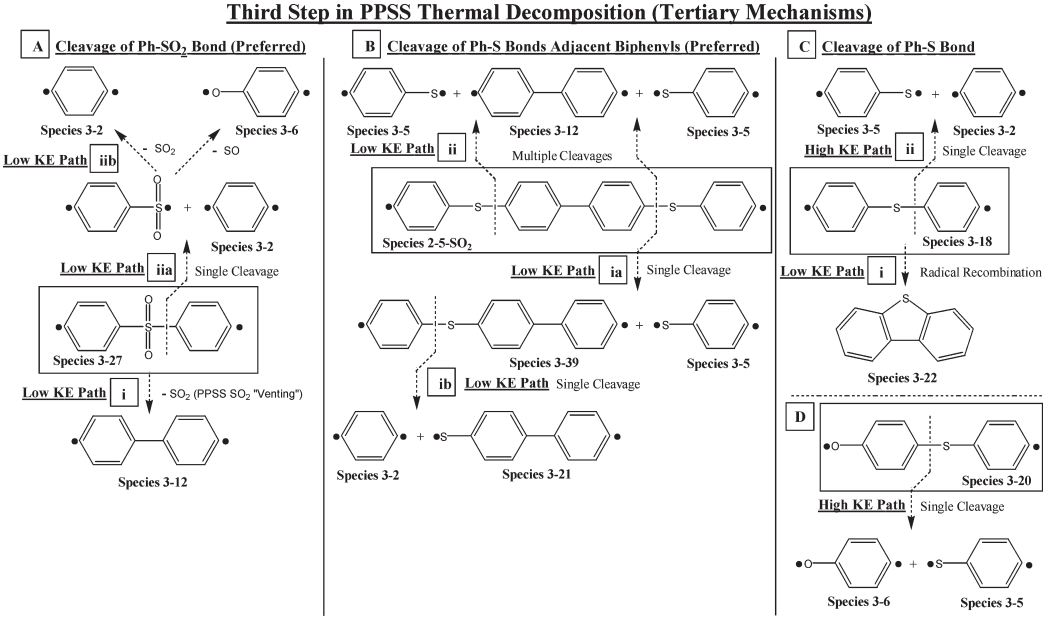

[a] Key: (A) Species 3-27 undergoes cleavage at only the Ph−SO_2 bond to produce (1) species 3-12 and (ii) species 3-2 and 3-6; (B) species 2-5-SO_2 can undergo a single main-chain fragment of the (ia) Ph−S bond to produce species 3-5 and 3-39 and (ib) species 3-2 and 3-21 or (ii) cleavage of multiple Ph−S bonds to yield fragment species 3-5 and 3-12; (C) species 3-18 can undergo (i) a radical recombination to produce species 3-22 or (ii) a single main-chain fragment of the Ph−S bond to produce species 3-2 and 3-5; and (D) species 3-20 can undergo a single main-chain fragment of the (i) Ph−S bond to produce species 3-5 and 3-6. All fragment species are observed in Figure 7.

the precursor ion. This indicates that the reactions shown in Scheme 2B are high energy pathways in which the oxygen atom can be retained by low mass fragment or completely expelled from the remaining fragments. Note that the formation of sulfoxide fragments was previously observed in our CID studies of PPSF.[12]

Pyrolysis−GC/MS. Pyrolysis products were identified using library matching software, where a match of 85% or greater was accepted. The following terminology will be used when relating the pyrolysis products shown in Table 3 with their peak intensities observed for the PPSS pyrogram shown in Figure 7: *major* (>50% base peak, BP); *medium* (30−50% BP); *small* (7−30% BP); *minor* (3−7% BP); and *trace* (<3% BP). In the following section, we will discuss the observed pyrolysis product peaks in decreasing order of peak intensity.

Pyrolysis is a higher energy bond fragmentation method than MS/MS. Thermal degradation of PPSS requires temperatures in excess of 650 °C, which is comparable with PSF at 700 °C.[11] This temperature is higher than that seen with PPS (500 °C),[13] owing to the fact that PPSS is a much more thermally stable polymer; however, PPSS is not as stable as PPSF where the lowest usable pyrolysis temperature was 800 °C.[12] It is also important to note that PPSS degradation may begin slightly above 650 °C, however, usable pyrograms, with appreciable amounts of characteristic PPSS pyrolysis products, are *not* obtained at temperatures below 900 °C. This relationship between set pyrolysis temperatures and usable programs is dependent upon the kinetic energy available to cleave bonds. As such, multiple bond-breaking reactions dominate in Py−GC/MS.

Also, when developing fragmentation mechanisms from polymer pyrolysis, two factors are important: (1) bond dissociation energies (the weakest bonds generally break first), and (2) stability of the generated radicals.[20] Using previously determined thermal degradation mechanisms for the structurally similar PSF[11] and PPS,[13,21] one can predict the order of bond breaking (weakest to strongest) for PPSS: Ph−SO_2, Ph−S, and Ph−Ph.

Similarities between MALDI−TOF/TOF CID Fragmentation and Py−GC/MS Data. Figure 7 displays programs of PPSS taken at 900 °C to show the pyrolysis composition at ideal pyrolysis temperatures. At higher set pyrolysis temperatures (above 1000 °C), excessive fragmentation occurs, limiting the information which can be obtained about the polymer. Scheme 3 shows the first step in the thermal decomposition of PPSS: the breaking of the Ph−SO_2 bond. MALDI−TOF/TOF CID has a much lower kinetic energy than Py−GC/MS, thus PPSS would initially break via Scheme 3A (single bond cleavages). Depending on the nature of the end-groups, this could result in the production of sulfur dioxide (species 3−1). However, under the high kinetic energy conditions of pyrolysis, at 900 °C, there will be multiple main-chain fractures and the initial fragments produced will be species 2−1, 2−5, and 3−1 (SO_2), as shown in Scheme 3B. It should be noted that sulfur dioxide (species 3−1) is always the major pyrolysis product (the base peak, BP; 100%), regardless of decomposition temperature. This can not only be explained by multiple main-chain fragmentation (Scheme 3B), but also by SO_2 "venting" from the PPSS main-chain (Scheme 3Aii) and SO_2 loss from fragment ion end groups (Scheme 3Aiii).[6] Unlike MALDI−TOF/TOF CID, the "pulse" of kinetic energy for Py−GC/MS has a much longer duration, thus allowing time for fragment species (e.g., species 2−1 and 2−5) to undergo further degradation reactions.

Scheme 4 shows the secondary mechanism in PPSS thermal decomposition: competition for main-chain scission at the Ph−SO_2 (Scheme 4A) vs Ph−S (Scheme 4B) bond. According to the BDEs for PPSS, species 2−5 should show preferential cleavage at

Table 3. Structural Assignments for Pyrolysis Products Observed in the Py−GC/MS Pyrograms reported in Figure 7

Species		Ret. Time (min)	Structure	M (Da) (* = no Na^+)	900 °C Peak Intensity (% Base Peak)
3-1	Sulfur Dioxide	1.02	SO_2	*64.0	100-major
3-22	Dibenzothiophene	15.78	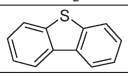	*184.0	34.9-medium
3-18	Diphenyl sulfide	13.84	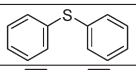	*186.1	32.9-medium
3-12	Biphenyl	11.22	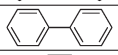	*154.2	32.5-medium
3-41	4-(Phenylthio)-diphenylsulfide	23.69	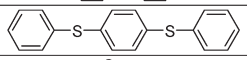	*294.1	26.8-small
3-34	4-Chlorodiphenyl sulfone	19.12	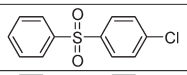	*252.0	25.4-small
3-23	4-Chlorodiphenyl sulfide	15.90	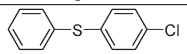	*220.0	25.1-small
3-39	4-Phenyl diphenylsulfide	22.15	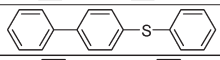	*262.1	22.9-small
3-25	Diphenyl disulfide	16.58	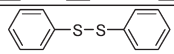	*218.0	20.9-small
3-19	4-Methyldiphenyl sulfide	15.11	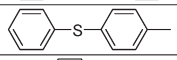	*200.1	19.4-small
3-5	Benzenethiol	4.73		*110.0	17.1-small
3-2	Benzene	1.37		*78.1	16.9-small
3-37	4,4'-Dichlorodiphenyl sulfone	20.55	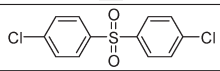	*286.0	15.7-small
3-9	4-Chlorobenzenethiol	7.64	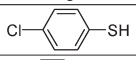	*144.0	15.4-small
3-4	Chlorobenzene	2.88		*112.7	15.0-small
3-6	Phenol	5.11		*94.1	12.9-small
3-7	1,3-Dichlorobenzene	5.49	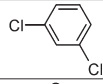	*146.0	11.2-small
3-27	Diphenyl sulfone	17.54	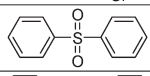	*218.0	7.8-small
3-14	Diphenylmethane	11.75	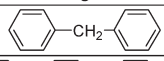	*168.1	7.2-small
3-38	4-Thiol-*p*-terphenyl	21.51	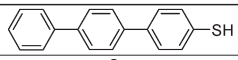	*262.1	6.6-minor
3-29	Bis(phenylthio)methane	17.87	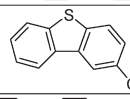	*218.0	6.4-minor
3-36	*p*-Terphenyl	20.14	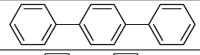	*230.1	6.4-minor
3-15	4-Methylbiphenyl	12.55		*168.2	6.2-minor
3-8	4-Methylbenzenethiol	6.02		*124.0	5.5-minor
3-21	Biphenylthiol	15.36	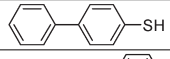	*186.1	4.9-minor
3-35	*m*-Terphenyl	19.76	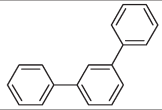	*230.1	4.9-minor
3-24	4,4'-Dichlorobiphenyl	16.00		*222.0	4.1-minor
3-10	4-Chlorophenol	8.45		*128.6	4.0-minor
3-3	Toluene	1.97		*92.1	3.7-minor
3-26	3-Methyl-dibenzothiophene	16.99	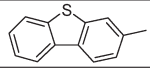	*198.1	3.4-minor

dx.doi.org/10.1021/ma200564f |*Macromolecules* 2011, 44, 5093–5104

Table 3. Continued

Species		Ret. Time (min)	Structure	M (Da) (* = no Na^+)	900 °C Peak Intensity (% Base Peak)
3-40	1-Phenylnaphtho(2,1-b)thiophene	22.87	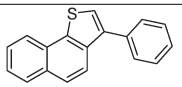	*260.1	3.4-minor
3-13	Diphenylether	11.35	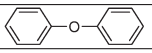	*170.2	3.0-minor
3-31	4-Chloro-4'-thiodiphenylsulfide	18.47	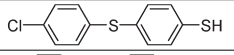	*252.0	2.9-trace
3-20	4-Hydroxydiphenyl sulfide	15.26	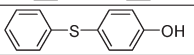	*202.1	2.6-trace
3-17	4-Chlorobiphenyl	13.66	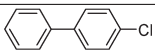	*188.0	2.5-trace
3-43	4-(4'-Methyl-biphenyl-4-ylsulfanyl)-benzenethiol	24.57	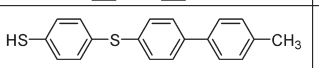	*308.1	2.5-trace
3-16	Dibenzofuran	12.83	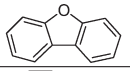	*168.1	2.3-trace
3-42	4-Phenyl diphenyl disulfide	24.05	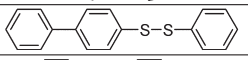	*294.1	2.1-trace
3-28	4-Thiodiphenylsulfide	17.60	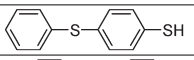	*218.0	2.0-trace
3-30	4,4'-Dichlorodiphenylsulfide	17.99	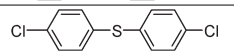	*254.0	2.0-trace
3-45	4-Hydroxy-4'-phenoxydiphenyl sulfone	25.55	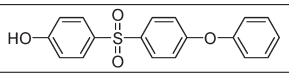	*326.1	1.2-trace
3-44	4-Chloro-4'-(Phenylthio)-diphenylsulfide	25.18	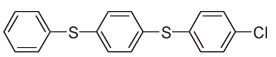	*328.0	1.1-trace
3-33	4-Benzenesulfonyl-benzenethiol	18.90	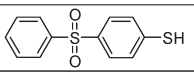	*250.0	1.0-trace
3-11	1,2-Benzenedithiol	9.75	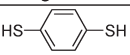	*142.0	0.8-trace
3-32	4-Methyldiphenyl sulfone	18.84	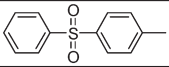	*232.1	0.8-trace
3-46	4-(Phenylthio)-diphenyl sulfone	26.38	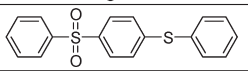	*326.0	0.3-trace
3-47	4-Chloro-4'-(Phenylthio)-diphenyl sulfone	28.00	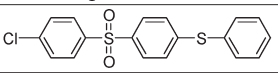	*360.0	0.2-trace

the Ph−SO_2 bond (Scheme 4A). An example of this is shown in Scheme 4Ai: intramolecular extrusion of SO_2 from the diphenyl sulfone group and concomitant formation of a biphenyl-linkage,[6] which will be referred to as SO_2 "venting." This process would result in the production of species 2−5-SO_2 or, in the case of MALDI−TOF/TOF CID, species 2−8. By a second low energy pathway, single cleavage at the Ph−SO_2 bond (Scheme 4Aiia) would produce species 3−18 (32.9% BP, *medium*) and a fragment similar to the TOF/TOF CID species 2−4, which can further degrade into species 3−18 and 3−20. There is another competing secondary mechanism: scission at the Ph−S bond (Scheme 4B). This is a high energy pathway that occurs when species 2−5 undergoes cleavage of a Ph−S bond, closest to the sulfone group, to produce species 3−5 and 3−46 (Scheme 4Bia) are produced. If a second Ph−S bond is cleaved in the 3−46 fragment (Scheme 4Bia), species 3−5 and 3−27 are formed. These cleavages could be induced by β-scission from phenyl radical migration to the position adjacent to the sulfur atom. An additional fragmentation pattern would be observed when species 2−5 undergoes multiple main-chain scissions of the Ph−S bonds (Scheme 4Bii) closest and farthest away from the sulfone group. This would result in the production of fragment species 3−2, 3−5, and 3−33.

At 900 °C and above, there is sufficient energy for fragment species 2−5-SO_2, 3−18, 3−20 and 3−27 to undergo additional degradation as shown in Scheme 5. Again, preferential cleavage should occur at the Ph−SO_2 bond. This is shown in Scheme 5A, in which species 3−27, a secondary product of Scheme 4Bi, can degrade into species 3−12 (32.5% BP, *medium*) through SO_2 "venting" (Scheme 5Ai) or undergo cleavage of the Ph−SO_2 bond (Scheme 5Aiia) to produce species 3−2 (16.9% BP, *small*), and an intermediate species which loses sulfur dioxide or sulfur monoxide (Scheme 5Aiib) to produce species 3−2 (17.1% BP, *small*) and 3−6 (12.9% BP, *small*), respectively. Scheme 5B presents a second low energy fragmentation pathway, *vide infra*. In this pathway, species 2−5-SO_2 can undergo cleavage at both the Ph−S bonds adjacent to the biphenyl-linkage. Cleavage of a single Ph−S bond (Scheme 5Bia) closest to the biphenyl group

dx.doi.org/10.1021/ma200564f |*Macromolecules* 2011, 44, 5093–5104

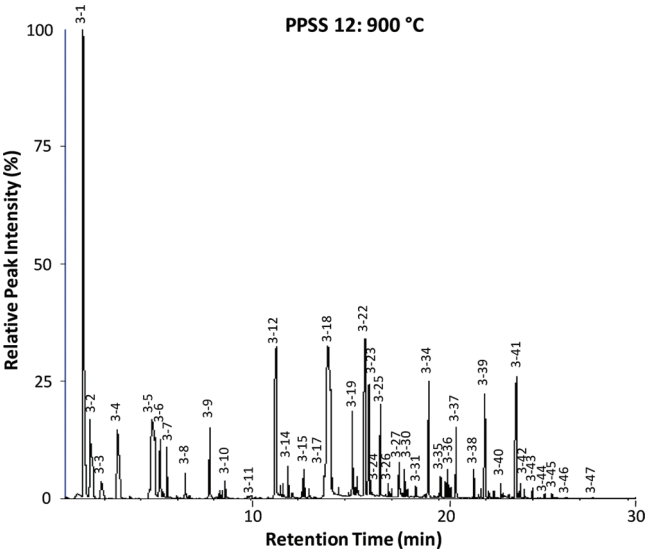

Figure 7. Py−GC/MS pyrograms of PPSS taken at 900 °C. Sample size: 0.5 mg.

produces species 3−5 (17.1% BP, *small*) and 3−39 (22.9% BP, *small*). Cleavage of the two Ph−S bonds (Scheme 5Bii) closest to the biphenyl group produces species 3−5 (17.1% BP, *small*) and 3−12 (32.5% BP, *medium*). Species 3−18 and 3−20, produced from both secondary fragmentations (Scheme 4A), can then undergo subsequent fragmentation, as shown in Scheme 5, parts C and D, respectively. Scheme 5C shows that species 3−18 can undergo a low energy radical recombination to form species 3−22 (34.9% BP, *medium*) or a high energy cleave at a Ph−S bond (presumably by β-scission) to form species 3−2 and 3−5. Additionally, Scheme 5D shows that once 3−20 is produced, the Ph−S bond can be cleaved to produce species 3−5 (17.1% BP, *small*) and 3−6 (12.9% BP, *small*).

Bond dissociation energies predict that cleavages of the Ph−SO_2 bonds will always be predominant over Ph−S bonds. However, this rule is no longer valid when a biphenyl-linkage is introduced into the PPSS fragment backbone. Combining this simple logic with Schemes 4 and 5, we can predict the most probable origin of the pyrolysis peaks in Figure 7. Since Scheme 4 does not contain species with biphenyl-linkages, we can apply the rule of Ph−SO_2 bond breaking predominance and conclude that species 3−18 (32.9% BP, *medium*) is the product of the secondary reaction shown in Schemes 4Aiia and 4Aiib. This logic would also appear to apply to the production of species 3−12 (32.5% BP, *medium*) in Scheme 5Ai; in addition to the radical reaction shown in Scheme 5Ci to produce species 3−22 (34.9% BP, *medium*). Now for the exception to the rule: Scheme 5B contains a PPSS compound with a biphenyl-linkage (species 2−5-SO_2). Because of the weakened Ph−S bonds adjacent to the biphenyl group, we must now assume that the reaction mechanisms shown in Scheme 5B makes a substantial contribution to the production of species 3−12 (32.5% BP, *medium*), 3−39 (22.9% BP, *small*), 3−5 (17.1% BP, *small*), 3−2 (16.9% BP, *small*), and 3-21 (4.9% BP, *minor*). However, these reaction mechanisms do not explain all of the peaks observed at the *small* level and above. There are other possibilities at pyrolysis temperatures of 900 °C: recombination reactions and sulfone reduction to sulfide can take place. For instance, species 3−7, 3−19, 3−25, and 3−37 can only be explained as being products of recombination reactions. While, species 3−9 and 3−41 appear to be the products of sulfone compounds being reduced to sulfide compounds; however, it is certainly possible that recombination reactions could have made a contribution to their peak intensities.

A number of "unexpected" sulfone-containing PPSS fragment species were identified using Py−GC/MS: 3−27, 3−32, 3−33, 3−34, 3−37, 3−45, 3−46, and 3−47. This observation is consistent with our previous Py−GC/MS study of PSF,[11] which identified "new" *sulfonated* compounds (at the *trace* level). (For PPSF, these sulfonated species were not seen; however, four sulfide-containing species were identified,[12] again at the *trace* level.) A majority of these sulfonated PPSS compounds were observed at the *trace* level (around 1%). With two exceptions: species 3−34 and 3−37, which yielded peak intensities of 25.4 and 15.7%, respectively. Previously studies on PES have identified sulfide degradation products, produced via reduction of the sulfone group by hydrogen atoms.[9,10,22] Because of the similarity between PES and PPSF, these same degradation mechanisms are expected to apply to PPSF as well. In contrast, the presence of the isopropylidene and sulfide groups in PSF and PPSS, respectively, may stabilize these polymers during degradation at higher temperatures; however, for PES and PPSF, the reduction of the sulfone group to the more stable sulfide moiety is necessary to achieve the same stability seen in PSF and PPSS.

CONCLUSIONS

The multimolecular free radical reactions in pyrolysis were compared with the unimolecular fragmentation reactions of MS/MS to establish fragmentation patterns for PPSS. Comparisons were made with the fragmentation of PSF and PPSF, two structurally similar polymers, to establish the generality of the proposed fragmentation pattern. Using CID fragmentation, we were able to identify the preferred fragmentation of the Ph−SO_2 bond in poly(arylsulfone), as well as low kinetic energy fragmentation pathways such as loss of SO_2 chain ends from PPSS fragments and SO_2 "venting" from the PPSS backbone. Other mechanisms of interest include the high KE pathways of chlorine end group loss and reduction of sulfone groups to sulfoxides and sulfides. Also, Py−GC/MS identified eight previously unobserved sulfone-containing fragments, two of which had only been previously identified in our recent studies on PSF.

ASSOCIATED CONTENT

Supporting Information. MALDI−TOF/TOF mass spectrum for linear PPSS. This material is available free of charge via the Internet at http://pubs.acs.org.

AUTHOR INFORMATION

Corresponding Author

*Telephone: (979) 238-1778. E-mail: APGies@Dow.com.

Present Addresses

‡Department of Core R&D Analytical Sciences, The Dow Chemical Company, 2301 N. Brazosport Blvd., B-1219, Freeport, TX 77541

⊥School of Law, University of Kansas, Lawrence, KS 66045

Notes

#Retired

■ ACKNOWLEDGMENT

We would like to thank Stephen L. Morgan for use of his Py−GC/MS instrument, Mitchell D. Refvik, Jim D. Byers, and JaNeille K. Dixon for their helpful synthesis advice, and Chevron Phillips Chemical Company, LP, for financial support.

■ REFERENCES

(1) El-hibri, M. J.; Nazabal, J.; Equiazabal, J. I.; Arzak, A. In *Handbook of Thermoplastics*; Olabisi, O., Ed.; Marcel Dekker: New York, 1997; pp 893−950.

(2) Clendinning, R. A.; Dickinson, B. L. In *Polymeric Materials Encyclopedia*; Salamone, J. C., Ed.; CRC Press: New York, 1996; pp 5562−5569.

(3) Almén, P.; Ericsson, I. *Polym. Degrad. Stab.* **1995**, *50*, 223–228.

(4) Botvay, A.; Mathe, A.; Poppl, L.; Rohonczy, J.; Kubatovicx, F. *J. Appl. Polym. Sci.* **1999**, *74*, 1–13.

(5) Lisa, G.; Avram, E.; Paduraru, G.; Irimia, M.; Hurduc, N.; Aelenei, N. *Polym. Degrad. Stab.* **2003**, *82*, 73–79.

(6) Montaudo, G.; Puglisi, C.; Rapisardi, R.; Samperi, F. *Macromol. Chem. Phys.* **1994**, *195*, 1225–1239.

(7) Montaudo, G.; Puglisi, C.; Samperi, F. *Macromol. Chem. Phys.* **1994**, *195*, 1241–1256.

(8) Ohtani, H.; Ishida, Y.; Ushiba, M.; Tsuge, S. *J. Anal. Appl. Pyrolysis* **2001**, *61*, 35–44.

(9) Perng, L. H. *J. Polym. Sci., Part A: Polym. Chem.* **2000**, *38*, 583–593.

(10) Perng, L. H. *J. Polym. Sci., Part A: Polym. Chem.* **2001**, *81*, 2387–2398.

(11) Ellison, S. T.; Gies, A. P.; Hercules, D. M.; Morgan, S. L. *Macromolecules* **2009**, *42*, 3005–3013.

(12) Ellison, S. T.; Gies, A. P.; Hercules, D. M.; Morgan, S. L. *Macromolecules* **2009**, *42*, 5526–5533.

(13) Gies, A. P.; Geibel, J. F.; Hercules, D. M. *Macromolecules* **2010**, *43*, 952–967.

(14) Gies, A. P.; Geibel, J. F.; Hercules, D. M. *Macromolecules* **2010**, *43*, 943–951.

(15) Edmonds, J. T.; Hill, H. W. Phillips Petroleum Co.: U.S. Patent 3,354,129, 1967.

(16) Yang, H. H. *Aromatic High-Strength Fibers*; John Wiley & Sons, Inc.: New York, 1989; p 873.

(17) Reentz, W. D.; Kaplan, M. L. *Polymer* **1982**, *23*, 310–313.

(18) Wade, B.; Abhiraman, A. S.; Wharry, S.; Sutherlin, D. *J. Polym. Sci., Part B: Polym. Phys.* **1990**, *28*, 1233–1249.

(19) Risch, B. G.; Srinivas, S.; Wilkes, G. L.; Geibel, J. F.; Ash, C. E.; White, S.; Hicks, M. *Polymer* **1996**, *37*, 3623–3636.

(20) Wampler, T. P. *Applied Pyrolysis Handbook*, 2nd ed.; CRC Press: Boca Raton, FL, 2007; pp 1−46.

(21) Geibel, J. F.; Campbell, R. W. In *Encyclopedia of Chemical Processing and Design*; McKetta, J. J., Cunningham, W. A., Eds.; Marcel Dekkar, Inc.: New York, 1992; Vol. 40, pp 94−125.

(22) Blazevska-Gilev, J.; Bastl, Z.; Subrt, J.; Stopka, P.; Pola, J. *Polym. Degrad. Stab.* **2009**, *94*, 196–200.